Supporting Information

# High-efficiency Fast-radiative Blue-emitting Perovskite Nanoplatelets and Their Formation Mechanisms

*Anqi Zhou, Yujun Xie, Feilong Wang, Rongqing Liang, Qiongrong Ou, and Shuyu Zhang**

Institute for Electric Light Sources, School of Information Science and Technology, Fudan University, Shanghai, 200433, P. R. China

E-mail: zhangshuyu@fudan.edu.cn

**Content:**

Figure S9. Images of $CsPbBr_3:Sb^{3+}$ NPL (a) solution and (b) film under ultraviolet excitation of 365 nm lamp.

Figure S10. A radar chart of high-quality blue-emitting perovskite NPLs in prior work and in our work for comparison.

Figure S11. Tauc plots of $(\alpha h\nu)^2$ against photon energy (eV) for $CsPbBr_3$:M NPLs/NCs.

Figure S12. Temperature dependence of the PL emission of $CsPbBr_3:Sb^{3+}$ NPLs with the temperature ranging from 78 to 298K.

Figure S13. One-dimensional $^1H$ spectrum of $CsPbBr_3$:M NPL/NC suspension in deuterated benzene ($C_6D_6$).

Figure S14. Nuclear Overhauser effect spectroscopy (NOESY) spectra of $CsPbBr_3$:M NPL/NC suspension in $C_6D_6$.

Figure S15. A schematic diagram of the perovskite model used in the calculation before and after growth.

Table S1. The inductively coupled plasma mass spectrometry (ICP-MS) analysis of $CsPbBr_3$:M (M=$Eu^{3+}$, $Sb^{3+}$, $Ba^{2+}$, $Zn^{2+}$) NPLs/NCs.

Table S2. Photoluminescence properties of pristine $CsPbBr_3$ and $CsPbBr_3$:M NPLs/NCs.

Table S3. A summary of optical performance of various blue-emitting perovskite NPLs.

## Experimental Section

*Materials*

Lead bromide ($PbBr_2$) 99.999% Aladdin; cesium bromide (CsBr) 99.99% Aladdin; oleic acid (OA) AR Aladdin; oleylamine (OLA) 80-90% Aladdin; N, N-Dimethylformamide (DMF) AR Sinopharm Group; $EuBr_3.xH_2O$ 99.99% Alfa Aesar; $SbBr_3.xH_2O$ 99.99% Alfa Aesar; $BaBr_2$ 99% Aladdin, $ZnBr_2$ 99% Aladdin; and methyl acetate (MeOAc) AR 98% Aladdin. The chemical reagents $EuBr_3.xH_2O$ and $SbBr_3.xH_2O$ used in this experiment need to be dried at 100℃ under vacuum for 12 hours to remove water before use. The other reagents were not further purified.

*Preparations of $CsPbBr_3$ NPLs/NCs Doped with Metal Ions*

We synthesized $CsPbBr_3$:M NPLs/NCs through an improved LARP scheme.[1, 2] First, 0.1 mmol $PbBr_2$, 0.1 mmol CsBr (and 0.15 mmol of doped metal salt for doped $CsPbBr_3$) were dissolved in 2.5 ml DMF solution and stirred at room temperature for 30 min. Next, an appropriate amount of OA (0.2 ml for pristine, $CsPbBr_3:Zn^{2+}$ and $CsPbBr_3:Eu^{3+}$, 0.19 ml for $CsPbBr_3:Ba^{2+}$ and 0.01 ml for $CsPbBr_3:Sb^{3+}$) and 0.125 ml OLA ligand were added and stirred at room temperature for 30 min to obtain a mixture precursor solution. Next, 0.5 ml of the precursor solution was quickly added dropwise into 5 ml of toluene and stirred at high speed for 30 s during this process, and then the fluorescent colloidal NPL/NC solution was obtained. Selecting $CsPbBr_3:Eu^{3+}$ as an example, 36.7 mg of $PbBr_2$, 21.3 mg of CsBr and 58.8 mg of $EuBr_3$ were dissolved in 2.5 ml DMF and stirred for 30 min. Next, 0.2 ml OA and

0.125 ml OLA ligand were added at room temperature and stirred for 30 min to obtain the precursor. Next, 0.5 ml of the precursor solution was quickly added dropwise into 5 ml of toluene and stirred for 30 s to obtain $CsPbBr_3$:$Eu^{3+}$ NPLs. The above operations are carried out under ambient environment.

To purify the prepared colloidal NPL/NC solutions, the prepared turbid solutions must first be centrifuged at 9,000 rpm for 10 min to remove the precipitated particles (aggregates) and to retain the supernatant with strong luminescence; MeOAc solvent was then added through a volume ratio of 1:1. After mixing, we removed the unreacted component and byproducts by centrifugation. Among them, $Eu^{3+}$-, $Sb^{3+}$- and $Ba^{2+}$-doped $CsPbBr_3$ NPLs are centrifuged at 12,000 rpm for 15 min, and $Zn^{2+}$-doped and pristine $CsPbBr_3$ NCs are centrifuged at 10,000 rpm for 10 min. After centrifugation, the supernatant that contains unreacted impurities and excess ligands was discarded, and the precipitate was redispersed in toluene or n-hexane solvent. The third purification was centrifuged at 6,000 rpm for 5 min to remove the precipitated particles that agglomerated during cleaning and that retained the supernatant.

*Characterizations*

The morphology (transmission electron microscope (TEM) and high-resolution transmission electron microscopy (HRTEM) images) and energy-dispersive X-ray spectroscopy (EDS) elemental mapping of perovskite NPLs/NCs were characterized by an FEI Tecnai G2 F20 operating at an accelerating voltage of 200 kV and equipped with a charge-coupled device camera (Quemese, EMSIS GmbH). The absorbance

spectra were measured by ultraviolet-visible (UV–Vis) spectroscopy (Purkinje, TU-1900). The PL spectra were recorded using an integrating sphere system equipped with a 360 nm continuous wave laser and a fiber-coupled spectrometer (Ocean Optics, QE Pro). photoluminescence quantum yield (PLQY), time-correlated single photon counting (TCSPC) and temperature-dependent PL spectra were measured by the Edinburgh FLS1000 integrated steady-state/transient fluorescence spectrometer system. The excitation light intensity was 365 nm, and the temperature range of temperature-dependent PL measurement was 78 K to 298 K, where the temperature interval was 20 K, and liquid nitrogen was used for cooling during the measurement. The lattice structure data of X-ray diffraction (XRD) analysis were collected by a Bruker D8 Advance diffractometer (Cu K-alpha radiation, lambda = 1.5418 Å). XPS analysis (Physical Electronics [PHI] 5300, 250 W, 12 kV) was performed on a PHI 5300 (250 W, 12 kV) using Al as the target anode. ICP–MS was carried out on a Thermo Fisher iCAP Q machine.

*NMR Measurements of $CsPbBr_3$:M NPL/NC Suspensions*

Pristine $CsPbBr_3$ and $CsPbBr_3$:M NPL/NC samples were prepared in $C_6D_6$ (D, 99.6% (0.03% v/v TMS)). All experiments were performed on a Bruker Avance NEO 700 spectrometer operating at a $^1H$ frequency of 700.23 MHz. The temperature was set to 298.0 K.

*Calculations for Electron Cloud Distribution, Electronic Structure and Energy Barriers*

It has been reported that Cs-terminated perovskites are more stable than Pb-terminated perovskites,[3] thus we selected Pb-terminated perovskites, which are relatively easy to grow[4], as an example. We assumed that CsBr is stacked on the original lead-rich surface, and then Cs atoms fix lead bromide to realize the complete growth of octahedron, simultaneously showing a transition state with 1/8 octahedron. Compared with the direct stacking octahedron reported in certain studies[5], this is the most fundamental elementary growth of perovskite. For actual calculation, a multiple-layer stacking structure was established with cells expanded 5 times and 3 times in two crystal directions. Periodic boundary conditions were applied, with the exception of the growth direction with an approximately 30 angstrom vacuum layer. All calculations were performed in CP2K[6]. Gaussian plane waves (GPW) in the QUICKSTEP module were employed with a double-zeta valence, polarized DZVP-MOLOPT-SR-GTH basis set[7] and norm-conserving, GTH-PBE pseudopotential[8]. A 500 Ry cutoff was applied for planewave expansion, and each Gaussian was mapped onto a 50 Ry cutoff grid. Dispersion with D3[9] was considered in all calculations. To speed up the operation, the orbital transformation (OT) method[10] was applied both in structural optimization and energy calculation. We optimized the initial structure for minimal energy. To maintain the consistency of Pb-octahedron after doping with different ions, the processes of structural relaxation, vibration and entropy change after reaching the transition state were disregarded.

In the process of thermodynamic calculation, Gibbs free energy is determined by enthalpy change, zero-point energy correction (ZPE) and entropy of the system, as shown in the following formula:

$$\Delta G = \Delta H + ZPE - T\Delta S \tag{S1}$$

ZPE is equivalent to the thermal correction of the internal energy at 0 k, and $\Delta S$ is calculated from the partition function. These two parts are computationally expensive in the existing structure system, so we used the calculation of $\Delta H$ instead of $\Delta G$ to reflect the lateral comparison of the doped and pristine $CsPbBr_3$ with each metal ion. Since the variation in $\Delta S$ induced by different doping conditions is small, the influence of this quantity in the lateral comparison can be disregarded. A negative value of $\Delta H$ appears in the calculation results, and the value of $\Delta G$ may obtain a positive potential barrier after the incorporation of the ZPE result, which may cancel out in the lateral comparison. Therefore, we considered the doping energy barrier in terms of the relative value of the energy change which controls the growth of NPLs (The absolute value is meaningless for judging the growth or lack of growth).

*Fitting of Exciton Binding Energy $E_b$*

The fitting was performed according to the following equation:

$$I(T) = \frac{I_0}{1 + Ae^{-E_b / k_B T} + Be^{-E_{trap} / k_B T}} \tag{S2}$$

where $A$ and $B$ are scale factors, $I_0$ is the integrated fluorescence intensity at 0 K, $k_B$ is Boltzmann's constant, $E_{trap}$ is the defect energy, and $E_b$ is the exciton binding energy.

The relationship between the radiative recombination rate $k_r$ and the exciton binding energy $E_b$ can be expressed as Formula (S3),[11]

$$k_r \propto F_{eff} = f_0 E_b \frac{\mu}{M} \frac{r(T)}{\Delta(T)} \quad \text{(S3)}$$

where $F_{eff}$ is the effective transition strength, $f_0$ is the dipole matrix element that connects Bloch states in the valance and conduction bands, $\mu$ is the reduced mass $\mu^{-1} = (m_e^*)^{-1} + (m_h^*)^{-1}$, $M = m_e^* + m_h^*$, $r(T)$ is the fraction of excitons within the spectral width $\Delta(T)$, and the enhanced exciton binding energy can effectively increase $k_r$, which is consistent with the $k_r$ results observed in the TCSPC measurement.

*Calculations for PLQY and Fluorescence Lifetime* $\tau_{ave}$

The high $k_r$ value thus contributes to improving PLQY and shortening the fluorescence lifetime through

$$\text{PLQY} = k_r / (k_r + k_{nr}) \quad \text{(S4)}$$

and

$$\tau_{ave} = (k_r + k_{nr})^{-1} \quad \text{(S5)}$$

formula.[12,13]

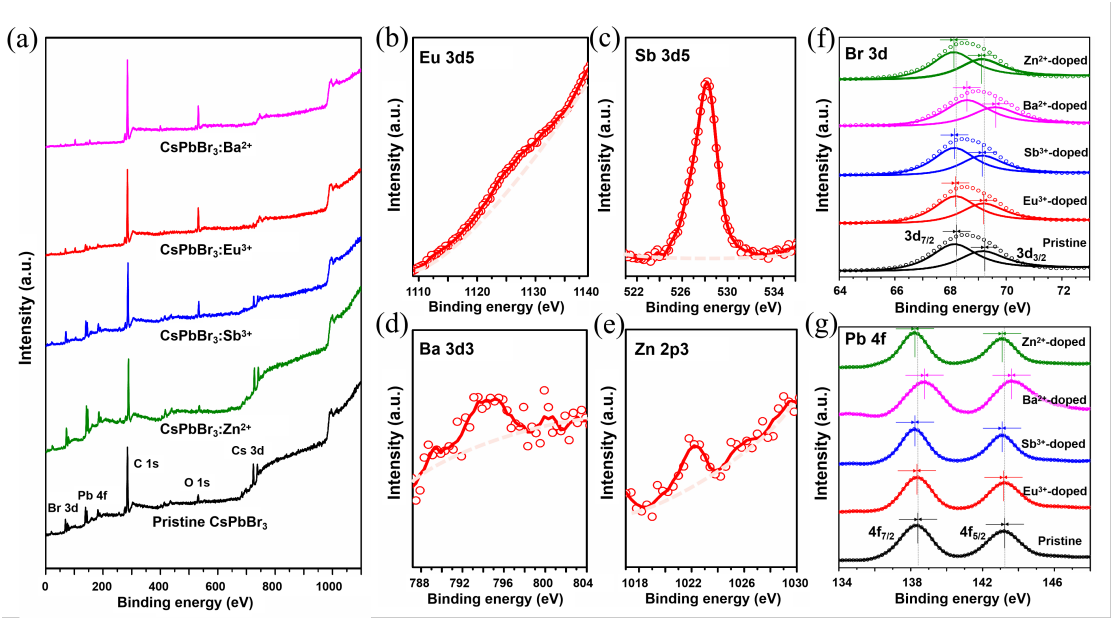


Figure S1. a) XPS spectra for the films of $CsPbBr_3$:M (M=$Eu^{3+}$, $Sb^{3+}$, $Ba^{2+}$, $Zn^{2+}$) NPLs/NCs and pristine $CsPbBr_3$ NCs. High-resolution XPS spectra corresponding to b) $Eu^{3+}$ 3d, c) $Sb^{3+}$ 3d, d) $Ba^{2+}$ 3d, e) $Zn^{2+}$ 2p, f) $Br^-$ 3d and g) $Pb^{2+}$ 4f, respectively. The hollow circular symbol represents the raw data and the solid curve represents the corresponding fitting curve. The dotted line represents the background curve.

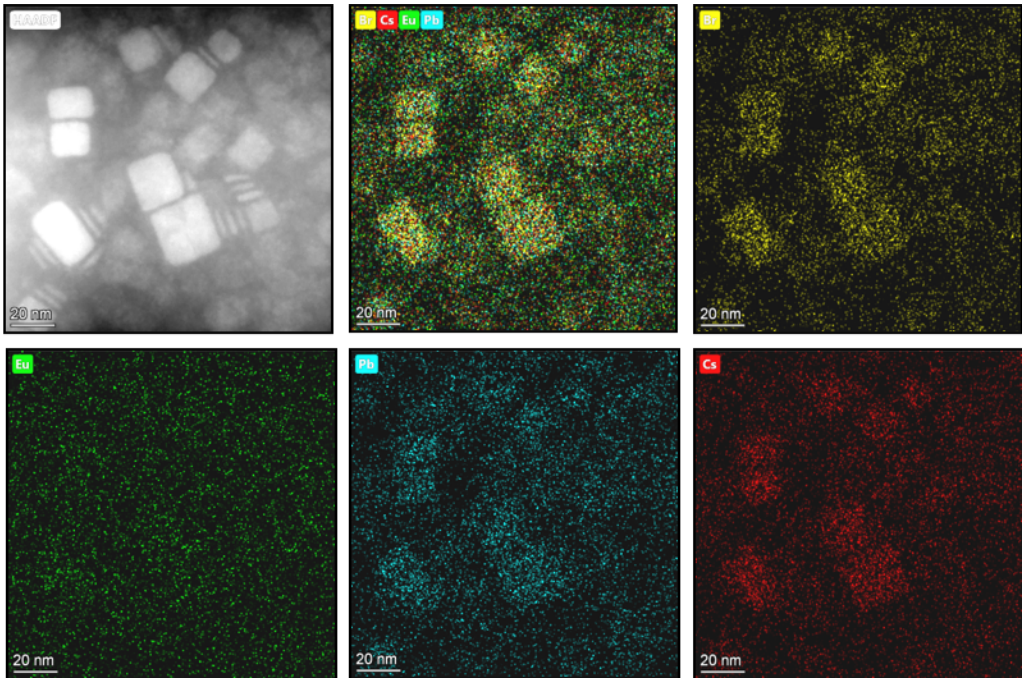


Figure S2. The HAADF-STEM image and elemental mappings of Cs, Pb, Eu, and Br elements in the $CsPbBr_3:Eu^{3+}$ NPLs. The second frame shows the overlap of the elemental mapping images.

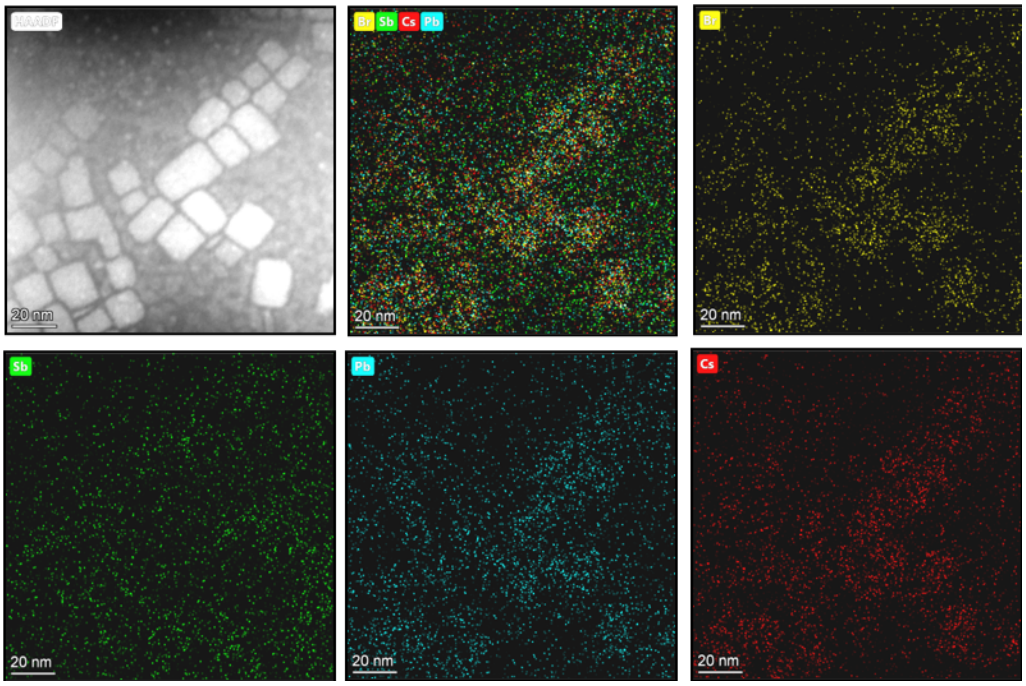


Figure S3. The HAADF-STEM image and elemental mappings of Cs, Pb, Sb, and Br elements in the $CsPbBr_3$:$Sb^{3+}$ NPLs. The second frame shows the overlap of the elemental mapping images.

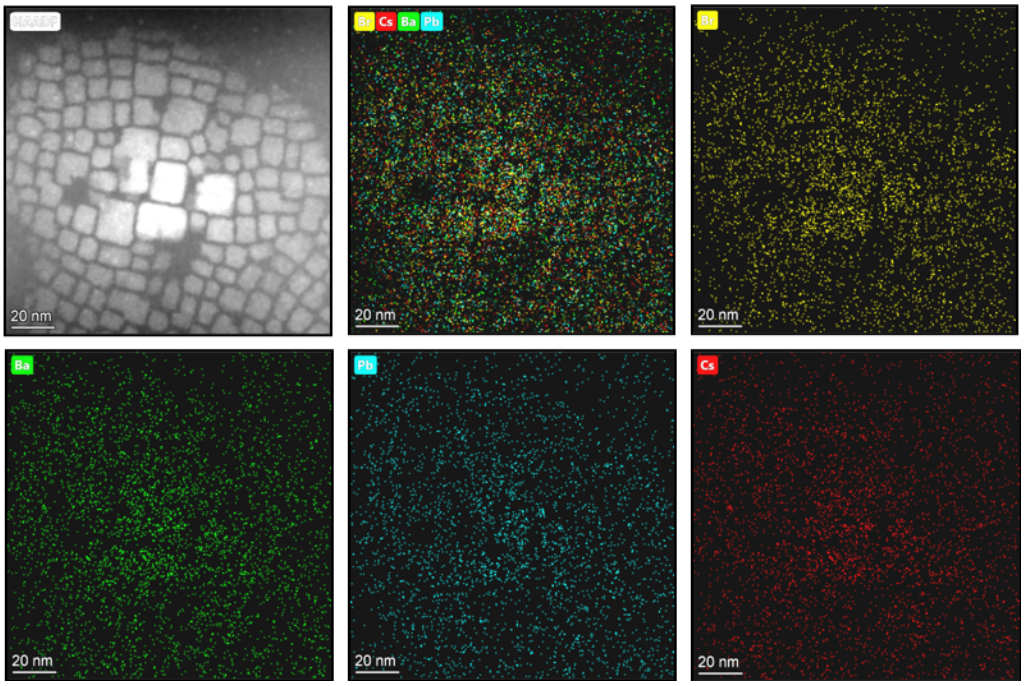


Figure S4. The HAADF-STEM image and elemental mappings of Cs, Pb, Ba, and Br elements in the $CsPbBr_3$:$Ba^{2+}$ NPLs. The second frame shows the overlap of the elemental mapping images.

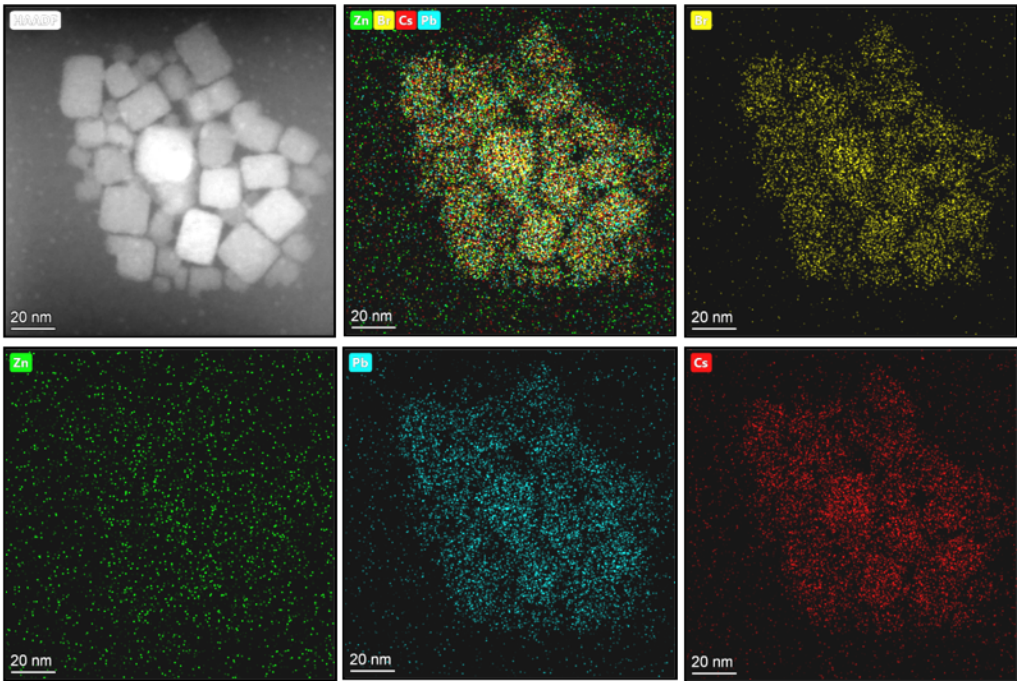


Figure S5. The HAADF-STEM image and elemental mappings of Cs, Pb, Zn, and Br elements in the $CsPbBr_3$:$Zn^{2+}$ NCs. The second frame shows the overlap of the elemental mapping images.

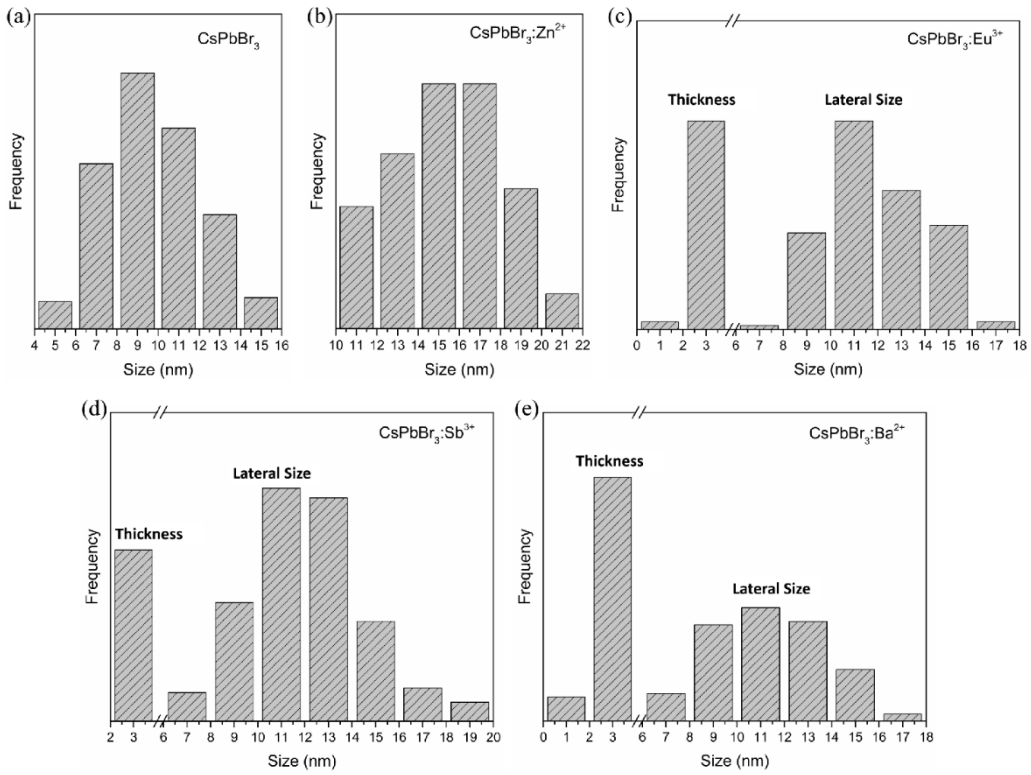


Figure S6. The size distribution statistics of (a) pristine $CsPbBr_3$ NCs, (b) $CsPbBr_3:Zn^{2+}$ NCs, (c) $CsPbBr_3:Eu^{3+}$ NPLs, (d) $CsPbBr_3:Sb^{3+}$ NPLs and (e) $CsPbBr_3:Ba^{2+}$ NPLs.

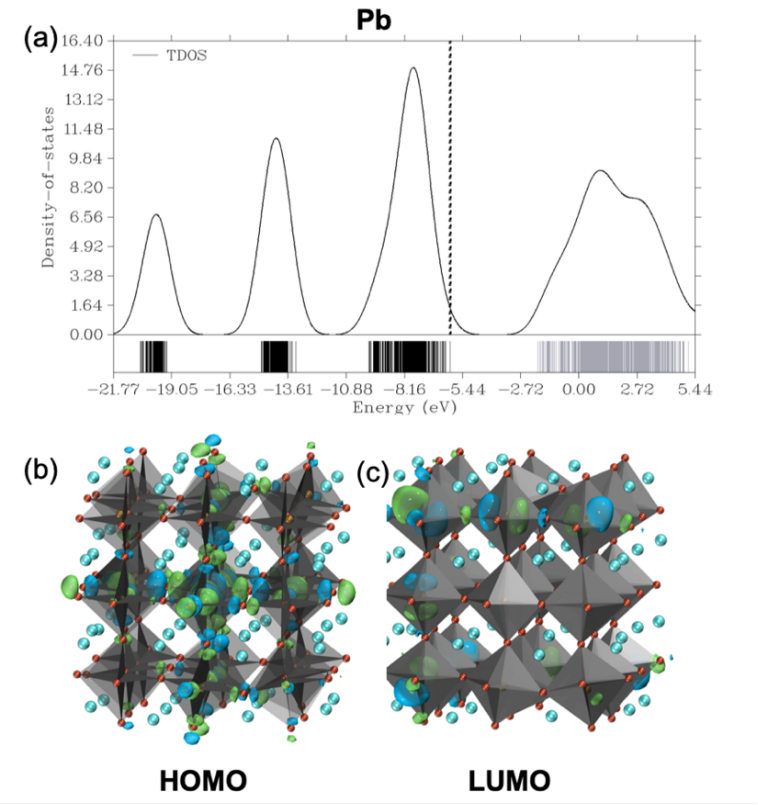


Figure S7. The electronic structure of pristine $CsPbBr_3$ NCs: (a) density of states, (b) HOMO and (c) LUMO in blue or green isosurface.

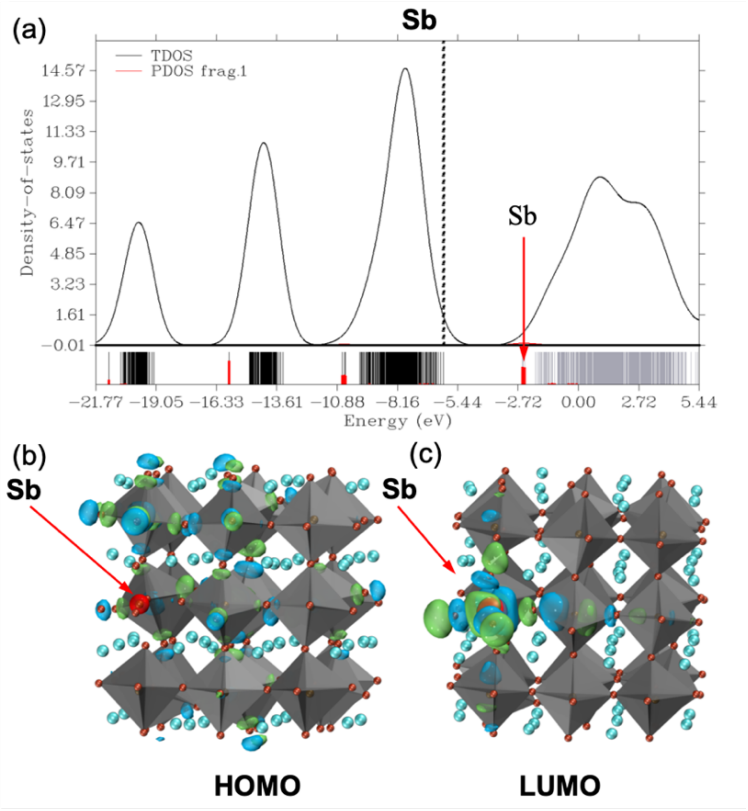


Figure S8. The electronic structure of $CsPbBr_3$:$Sb^{3+}$ NPLs: (a) density of states, (b) HOMO and (c) LUMO in blue or green isosurface.

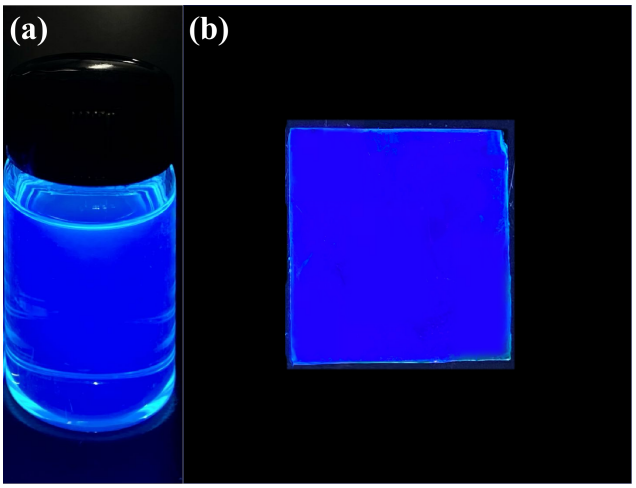


Figure S9. Images of $CsPbBr_3:Sb^{3+}$ NPLs in (a) solution and (b) film under ultraviolet (UV) excitation of 365 nm lamp.

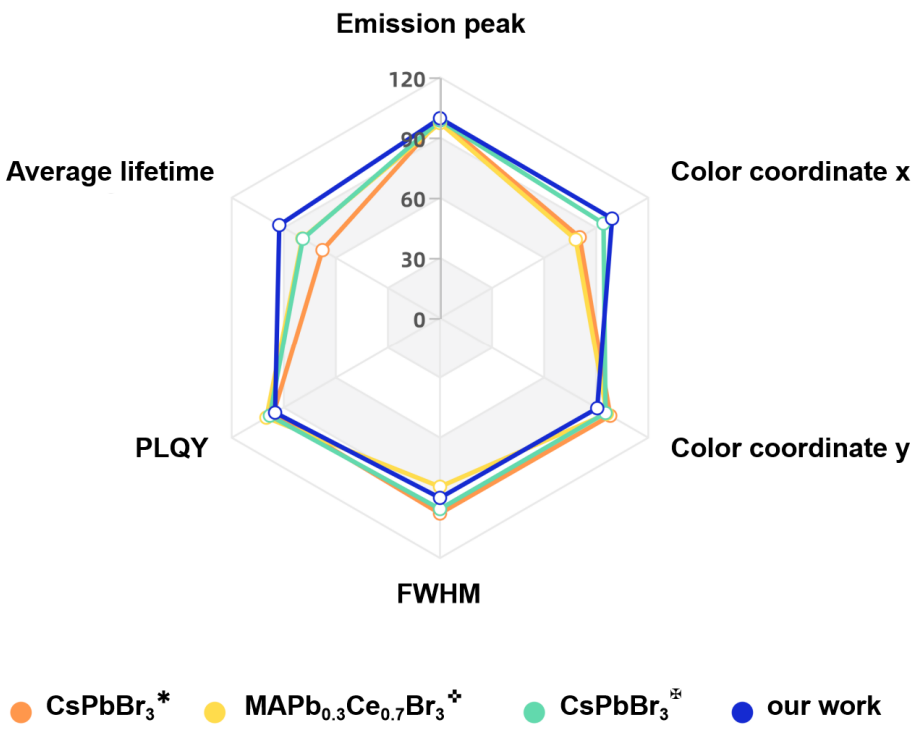


Figure S10. A radar chart of high-quality blue-emitting perovskite NPLs in prior work and in our work for comparison, showing properties of emission peak, color-coordinate x and y, full width at half maximum (FWHM), PLQY, and average lifetime. The references corresponding to each mark in the figure are: [✱] ACS Energy Lett. 2018, 3 (9), 2030-2037, [✣] J. Mater. Chem. C 2021, 9 (7), 2437-2454, [✠] Chem. Eng. J. 2021, 419, 129612.

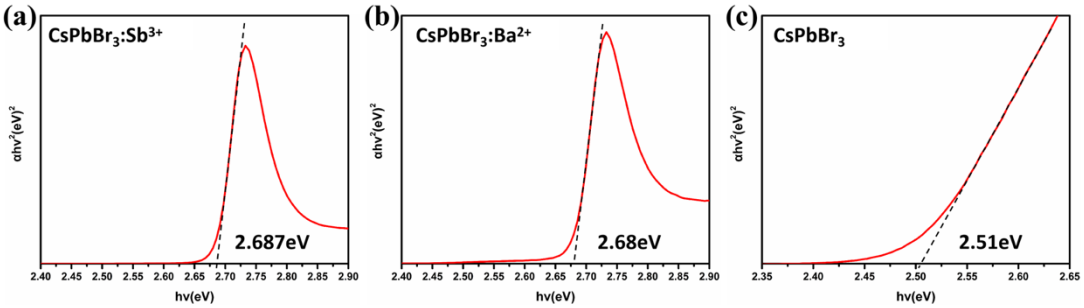


Figure S11. Tauc plots of $(\alpha h\nu)^2$ against photon energy (eV) for $CsPbBr_3$:M: (a) $Sb^{3+}$-, (b) $Ba^{2+}$- doped NPLs, and (c) pristine $CsPbBr_3$ NCs.

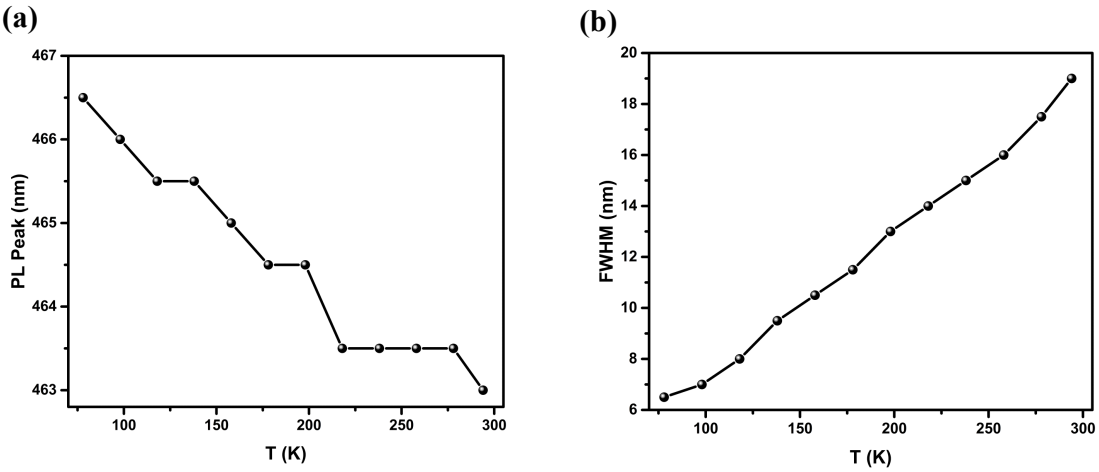


Figure S12. Temperature dependence of (a) the PL emission peak position, and of (b) linewidth (FWHM) of the PL emission of $CsPbBr_3$:$Sb^{3+}$ NPLs with the temperature ranging from 78 to 298K.

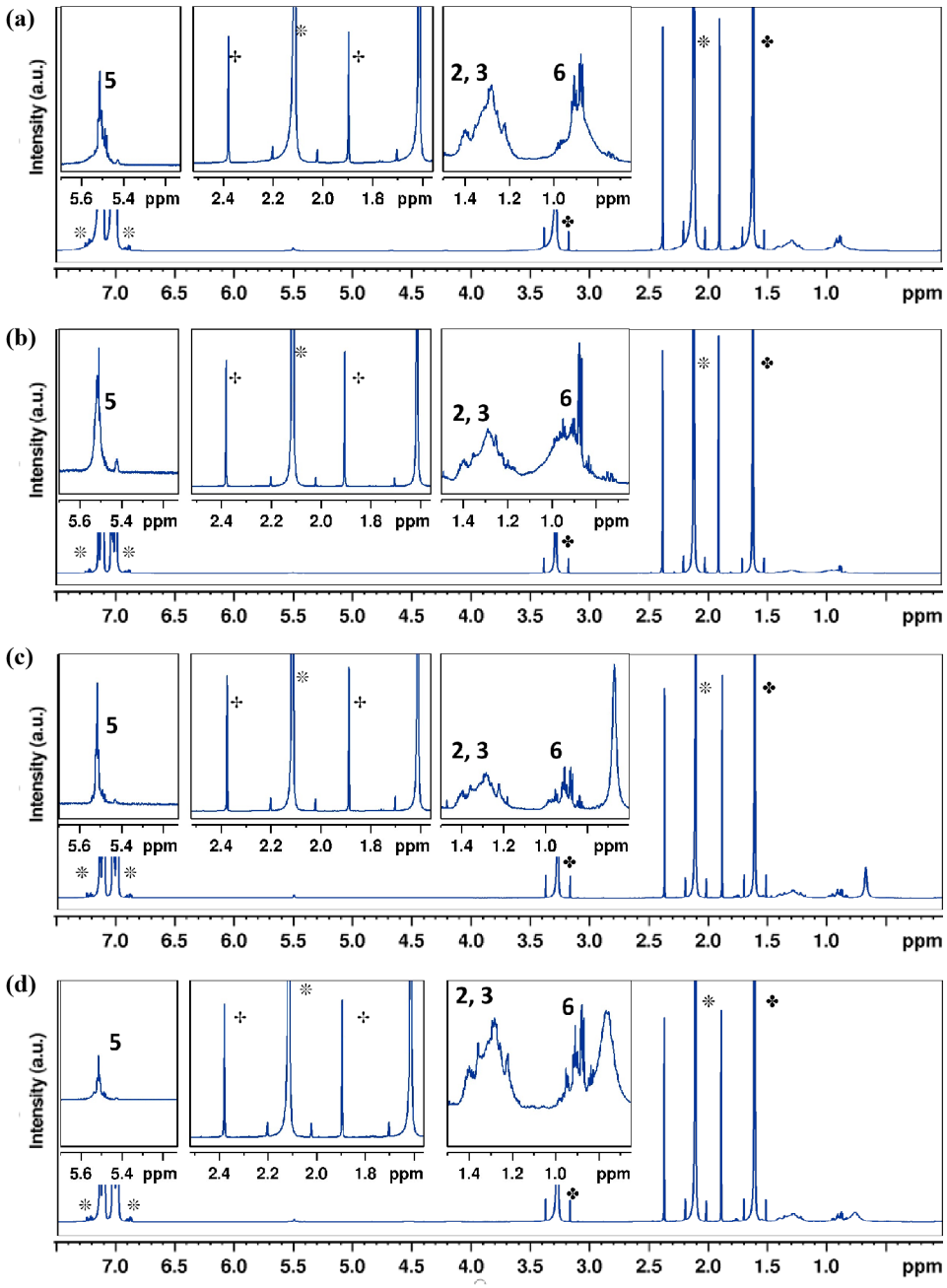


Figure S13. One-dimensional $^{1}H$ spectrum of (a) $CsPbBr_3:Zn^{2+}$ NC, (b) $CsPbBr_3:Sb^{3+}$ NPL, (c) $CsPbBr_3:Ba^{2+}$ NPL, and (d) $CsPbBr_3:Eu^{3+}$ NPL suspension in $C_6D_6$, and calibrated at 7.16 ppm. The residual solvent resonance peaks of toluene (✳), MeOAc(✤), and DMF(✢) are identified. The insets show the locally enlarged spectrum of corresponding figures.

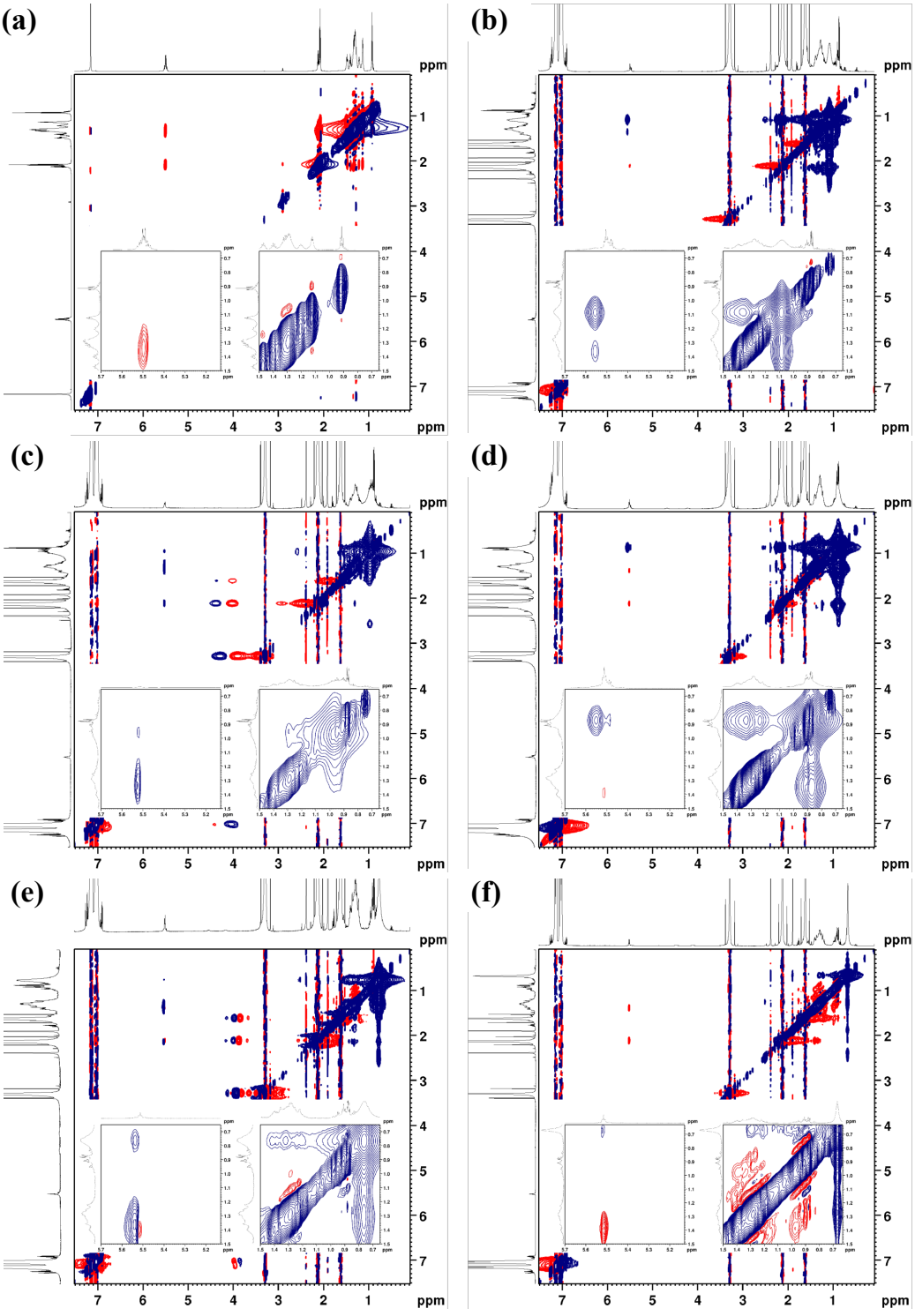


Figure S14. NOESY spectra of (a) pure OA, (b) pristine $CsPbBr_3$ NCs, (c) $Sb^{3+}$-doped $CsPbBr_3$ NPLs, (d) $Zn^{2+}$-doped $CsPbBr_3$ NCs, (e) $Eu^{3+}$-doped $CsPbBr_3$ NPLs, and (f) $Ba^{2+}$-doped $CsPbBr_3$ NPLs in suspension (dispersed in $C_6D_6$). For a better view, part of the NOESY spectrum are magnified to show the bound ligands in the inset.

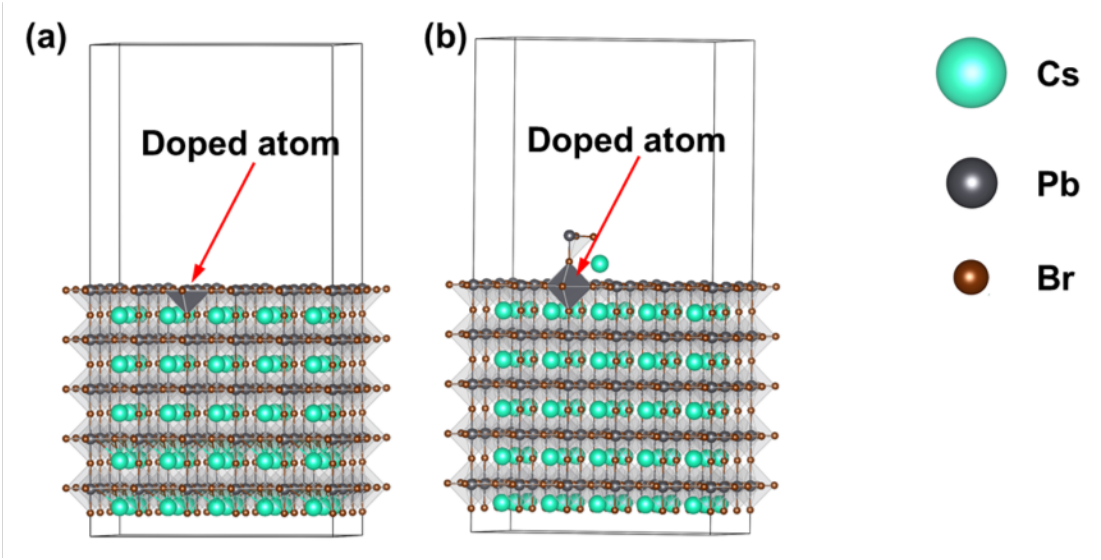


Figure S15. A schematic diagram of the perovskite model used in the calculation (a) before and (b) after growth.

Table S1. ICP-MS analysis of $CsPbBr_3$:M (M=$Eu^{3+}$, $Sb^{3+}$, $Ba^{2+}$, $Zn^{2+}$) NPLs/NCs.

| Samples | Elemets | μg/L | Mass fraction/(%) | μmol/L | M atomic doping ratio x=M/(Pb+M) |
|---|---|---|---|---|---|
| $CsPbBr_3:Eu^{3+}$ | Br | 4788.9 | 48.98 | 59.94 | Eu 1.8% |
| | Cs | 1389.8 | 14.22 | 10.46 | |
| | Eu | 48.1 | 0.49 | 0.32 | |
| | Pb | 3549.9 | 36.31 | 17.13 | |
| $CsPbBr_3:Sb^{3+}$ | Br | 4003.6 | 27.71 | 50.11 | Sb 3.2% |
| | Cs | 3636.7 | 25.17 | 27.36 | |
| | Pb | 6681.8 | 46.24 | 32.25 | |
| | Sb | 127.9 | 0.89 | 1.05 | |
| $CsPbBr_3:Ba^{2+}$ | Br | 5920.3 | 33.17 | 74.10 | Ba 2.6% |
| | Cs | 3315.8 | 18.58 | 24.95 | |
| | Ba | 152.1 | 0.85 | 1.11 | |
| | Pb | 8460.9 | 47.40 | 40.83 | |
| $CsPbBr_3:Zn^{2+}$ | Zn | 69.8 | 0.28 | 1.07 | Zn 2.8% |
| | Br | 12972.9 | 51.80 | 162.36 | |
| | Cs | 4371.4 | 17.46 | 32.89 | |
| | Pb | 7629.3 | 30.46 | 36.82 | |

Table S2. Photoluminescence properties of pristine $CsPbBr_3$ NCs and $CsPbBr_3$:M NPLs/NCs.

| Samples | Emission peak (nm) | FWHM (nm) | PLQY(S3*) |
|---|---|---|---|
| $CsPbBr_3$ | 504 | 25 | 63% |
| $CsPbBr_3:Zn^{2+}$ | 513 | 22 | 78% |
| $CsPbBr_3:Sb^{3+}$ | 465 | 19 | 95% |
| $CsPbBr_3:Eu^{3+}$ | 463 | 16 | 67% |
| $CsPbBr_3:Ba^{2+}$ | 463 | 19 | 69% |

* The PLQY measurements are implemented after the third recycling of purification of the as-synthesized NPLs/NCs.

Table S3. A summary of optical performance of various blue-emitting perovskite NPLs.

| Samples | Emission peak (nm) | FWHM (nm) | PLQY | Average lifetime (ns) | References |
|---|---|---|---|---|---|
| $MAPbBr_3$ | 469 | - | 12% | - | 2015[14] |
| $CsPbBr_3$ | 488 | 15 | 84% | - | 2015[15] |
| $CsPbBr_3$ | 459 | 19 | 31% | 3 | 2016[16] |
| $CsPbBr_3$ | 456 | 13 | 33% | 4.3 | 2016[17] |
| $FAPbBr_3$ | 439 | 11 | 22% | - | 2016[18] |
| $CsPbBr_3$ | 481 | 20.3 | 38% | - | 2018[19] |
| | 484 | 20.8 | 43% | - | |
| | 492 | 22.8 | 50% | - | |
| $CsPbBr_3$ | 452 | 11 | 60% | 4.1 | 2018[20] |
| | 432 | 11 | 49% | 4.0 | |
| $CsPbBr_3$ | 462 | 12 | 96% | 6.46 | 2018[21] |
| $CsPbBr_3$ | 460 | 16 | 14% | - | 2019[22] |
| | 487 | 25 | 17% | - | |
| $CsPbBr_3$ | 443, 462 | - | 50% | 5.3 | 2019[23] |
| $CsPbBr_3$ | 455 | 18 | 38% | - | 2020[24] |
| $CsPbBr_3$ | 450 | 15 | 40% | 3.68 | 2020[25] |
| $MAPb_{0.3}Ce_{0.7}Br_3$ | 454 | 24 | 100% | 4.14 | 2021[26] |
| $CsPbBr_3$ | 450 | - | 87% | 8.85 | 2021[27] |
| $CsPbBr_3$ | 460 | 14 | 98% | 4.2 | 2021[28] |
| $CsPbBr_3:xSb^{3+}$ (x=3.2%) | 465 | 19 | 95% | 1.48 | This work |

References:

1. Hintermayr, V. A.; Richter, A. F.; Ehrat, F.; Döblinger, M.; Vanderlinden, W.; Sichert, J. A.; Tong, Y.; Polavarapu, L.; Feldmann, J.; Urban, A. S., Tuning the Optical Properties of Perovskite Nanoplatelets through Composition and Thickness by Ligand-Assisted Exfoliation. *Adv. Mater.* **2016,** *28* (43), 9478-9485.

2. Zhang, F.; Zhong, H.; Chen, C.; Wu, X.; Hu, X.; Huang, H.; Han, J.; Zou, B.; Dong, Y., Brightly Luminescent and Color-Tunable Colloidal $CH_3NH_3PbX_3$ (X = Br, I, Cl) Quantum Dots: Potential Alternatives for Display Technology. *ACS Nano* **2015,** *9* (4), 4533-4542.

3. Chen, Y.; Smock, S. R.; Flintgruber, A. H.; Perras, F. A.; Brutchey, R. L.; Rossini, A. J., Surface Termination of $CsPbBr_3$ Perovskite Quantum Dots Determined by Solid-State NMR Spectroscopy. *J. Am. Chem. Soc.* **2020,** *142* (13), 6117-6127.

4. Yin, J.; Yang, H.; Gutiérrez-Arzaluz, L.; Zhou, Y.; Brédas, J.-L.; Bakr, O. M.; Mohammed, O. F., Luminescence and Stability Enhancement of Inorganic Perovskite Nanocrystals via Selective Surface Ligand Binding. *ACS Nano* **2021,** *15* (11), 17998-18005.

5. Cao, Q.; Ilyas, A.; Zhang, S.; Ju, Z.; Sun, F.; Liu, T.; Yang, Y.; Lu, Y.; Liu, X.; Deng, R., Lanthanide-doping Enables Kinetically Controlled Growth of Deep-blue Two-monolayer Halide Perovskite Nanoplatelets. *Nanoscale* **2021,** *13* (26), 11552-11560.

6. Kühne, T. D.; Iannuzzi, M.; Del Ben, M.; Rybkin, V. V.; Seewald, P.; Stein, F.; Laino, T.; Khaliullin, R. Z.; Schütt, O.; Schiffmann, F.; Golze, D.; Wilhelm, J.; Chulkov, S.; Bani-Hashemian, M. H.; Weber, V.; Borštnik, U.; Taillefumier, M.; Jakobovits, A. S.; Lazzaro, A.; Pabst, H.; Müller, T.; Schade, R.; Guidon, M.; Andermatt, S.; Holmberg, N.; Schenter, G. K.; Hehn, A.; Bussy, A.; Belleflamme, F.; Tabacchi, G.; Glöß, A.; Lass, M.; Bethune, I.; Mundy, C. J.; Plessl, C.; Watkins, M.; VandeVondele, J.; Krack, M.; Hutter, J., CP2K: An Electronic Structure and Molecular Dynamics Software Package - Quickstep: Efficient and Accurate Electronic Structure Calculations. *J. Chem. Phys.* **2020,** *152* (19), 194103.

7. VandeVondele, J.; Hutter, J., Gaussian Basis Sets for Accurate Calculations on Molecular Systems in Gas and Condensed Phases. *J. Chem. Phys.* **2007,** *127* (11), 114105.

8. Krack, M., Pseudopotentials for H to Kr Optimized for Gradient-corrected Exchange-correlation Functionals. *Theor. Chem. Acc.* **2005,** *114* (1), 145-152.

9. Grimme, S.; Antony, J.; Ehrlich, S.; Krieg, H., A Consistent and Accurate ab initio Parametrization of Density Functional Dispersion Correction (DFT-D) for the 94 Elements H-Pu. *J. Chem. Phys.* **2010,** *132* (15), 154104.

10. VandeVondele, J.; Hutter, J., An Efficient Orbital Transformation Method for Electronic Structure Calculations. *J. Chem. Phys.* **2003,** *118* (10), 4365-4369.

11. Feldmann, J.; Peter, G.; Göbel, E. O.; Dawson, P.; Moore, K.; Foxon, C.; Elliott, R. J., Linewidth Dependence of Radiative Exciton Lifetimes in Quantum Wells. *Phys. Rev. Lett.* **1987,** *59* (20), 2337-2340.

12. Tong, Y.; Ehrat, F.; Vanderlinden, W.; Cardenas-Daw, C.; Stolarczyk, J. K.; Polavarapu, L.; Urban, A. S., Dilution-Induced Formation of Hybrid Perovskite Nanoplatelets. *ACS Nano* **2016,** *10* (12), 10936-10944.

13. Vonk, S. J. W.; Fridriksson, M. B.; Hinterding, S. O. M.; Mangnus, M. J. J.; van Swieten, T. P.; Grozema, F. C.; Rabouw, F. T.; van der Stam, W., Trapping and Detrapping in Colloidal Perovskite Nanoplatelets: Elucidation and Prevention of Nonradiative Processes through Chemical Treatment. *J. Phys. Chem. C* **2020,** *124* (14), 8047-8054.

14. Sichert, J. A.; Tong, Y.; Mutz, N.; Vollmer, M.; Fischer, S.; Milowska, K. Z.; Cortadella, G. R.; Nickel, B.; Cardenas-Daw, C.; Stolarczyk, J. K.; Urban, A. S.; Feldmann, J., Quantum Size Effect in Organometal Halide Perovskite Nanoplatelets. *Nano Lett.* **2015,** *15* (10), 6521-6527.

15. Bekenstein, Y.; Koscher, B. A.; Eaton, S. W.; Yang, P.; Alivisatos, A. P., Highly Luminescent Colloidal Nanoplates of Perovskite Cesium Lead Halide and Their Oriented Assemblies. *J. Am. Chem. Soc.* **2015,** *137* (51), 16008-16011.

16. Akkerman, Q. A.; Motti, S. G.; Srimath K. A. R.; Mosconi, E.; D'Innocenzo, V.; Bertoni, G.; Marras, S.; Kamino, B. A.; Miranda, L.; De Angelis, F.; Petrozza, A.; Prato, M.; Manna, L., Solution Synthesis Approach to Colloidal Cesium Lead Halide

Perovskite Nanoplatelets with Monolayer-Level Thickness Control. *J. Am. Chem. Soc.* **2016,** *138* (3), 1010-1016.

17. Shamsi, J.; Dang, Z.; Bianchini, P.; Canale, C.; Di Stasio, F.; Brescia, R.; Prato, M.;Manna, L., Colloidal Synthesis of Quantum Confined Single Crystal $CsPbBr_3$ Nanosheets with Lateral Size Control up to the Micrometer Range. *J. Am. Chem. Soc.* **2016,** *138* (23), 7240-7243.

18. Weidman, M. C.; Seitz, M.; Stranks, S. D.; Tisdale, W. A., Highly Tunable Colloidal Perovskite Nanoplatelets through Variable Cation, Metal, and Halide Composition. *ACS Nano* **2016,** *10* (8), 7830-7839.

19. Zhao, J.; Cao, S.; Li, Z.; Ma, N., Amino Acid-Mediated Synthesis of CsPbBr3 Perovskite Nanoplatelets with Tunable Thickness and Optical Properties. *Chem. Mater.* **2018,** *30* (19), 6737-6743.

20. Bohn, B. J.; Tong, Y.; Gramlich, M.; Lai, M. L.; Döblinger, M.; Wang, K.; Hoye, R. L. Z.; Müller-Buschbaum, P.; Stranks, S. D.; Urban, A. S.; Polavarapu, L.; Feldmann, J., Boosting Tunable Blue Luminescence of Halide Perovskite Nanoplatelets through Postsynthetic Surface Trap Repair. *Nano Lett.* **2018,** *18* (8), 5231-5238.

21. Wu, Y.; Wei, C.; Li, X.; Li, Y.; Qiu, S.; Shen, W.; Cai, B.; Sun, Z.; Yang, D.; Deng, Z.; Zeng, H., In Situ Passivation of $PbBr_6^{4-}$ Octahedra toward Blue Luminescent $CsPbBr_3$ Nanoplatelets with Near 100% Absolute Quantum Yield. *ACS Energy Lett.* **2018,** *3* (9), 2030-2037.

22. Hoye, R. L. Z.; Lai, M.-L.; Anaya, M.; Tong, Y.; Gałkowski, K.; Doherty, T.; Li, W.; Huq, T. N.; Mackowski, S.; Polavarapu, L.; Feldmann, J.; MacManus-Driscoll, J. L.; Friend, R. H.; Urban, A. S.; Stranks, S. D., Identifying and Reducing Interfacial Losses to Enhance Color-Pure Electroluminescence in Blue-Emitting Perovskite Nanoplatelet Light-Emitting Diodes. *ACS Energy Letters* **2019,** *4* (5), 1181-1188.

23. Bi, C.; Wang, S.; Kershaw, S. V.; Zheng, K.; Pullerits, T.; Gaponenko, S.; Tian, J.; Rogach, A. L., Spontaneous Self-Assembly of Cesium Lead Halide Perovskite Nanoplatelets into Cuboid Crystals with High Intensity Blue Emission. *Advanced Science* **2019,** *6* (13), 1900462.

24. Peng, S.; Wei, Q.; Wang, B.; Zhang, Z.; Yang, H.; Pang, G.; Wang, K.; Xing, G.; Sun, X. W.; Tang, Z., Suppressing Strong Exciton–Phonon Coupling in Blue Perovskite Nanoplatelet Solids by Binary Systems. *Angew. Chem. Int. Ed.* **2020,** *59* (49), 22156-22162.

25. Shamsi, J.; Kubicki, D.; Anaya, M.; Liu, Y.; Ji, K.; Frohna, K.; Grey, C. P.; Friend, R. H.; Stranks, S. D., Stable Hexylphosphonate-Capped Blue-Emitting Quantum-Confined $CsPbBr_3$ Nanoplatelets. *ACS Energy Letters* **2020,** *5* (6), 1900-1907.

26. Parveen, S.; Prasanna, P. K.; Chakraborty, S.; Giri, P. K., Stable Deep Blue Emission with Unity Quantum Yield in Organic–inorganic Halide Perovskite 2D Nanosheets Doped with Cerium and Terbium at High Concentrations. *J. Mater. Chem. C* **2021,** *9* (7), 2437-2454.

27. Lin, H.; Wei, Q.; Ng, K. W.; Dong, J.-Y.; Li, J.-L.; Liu, W.-W.; Yan, S.-S.; Chen, S.; Xing, G.-C.; Tang, X.-S.; Tang, Z.-K.; Wang, S.-P., Stable and Efficient Blue-Emitting $CsPbBr_3$ Nanoplatelets with Potassium Bromide Surface Passivation. *Small* **2021,** *17* (43), 2101359.

28. Su, S.; Tao, J.; Sun, C.; Xu, D.; Zhang, H.; Wei, T.; Zhang, Z.-H.; Wang, Z.; Fan, C.; Bi, W., Stable and Highly Efficient Blue-emitting $CsPbBr_3$ Perovskite Nanomaterials via Kinetic-controlled Growth. *Chem. Eng. J.* **2021,** *419*, 129612.